

# Role of Energy Offset in Nonradiative Voltage Loss in Organic Solar Cells

Toshiharu Saito, Shin-ichiro Natsuda, Kenta Imakita, Yasunari Tamai,\*  
and Hideo Ohkita

The voltage loss incurred by nonradiative charge recombination should be reduced to further improve the power conversion efficiency of organic solar cells (OSCs). This work discusses the nonradiative voltage loss in OSCs with systematically controlled energy offset between optical bandgap and charge transfer (CT) states. It is demonstrated that the nonradiative voltage loss is a function of the energy offset; it drops sharply with decreasing energy offset. By measuring the quantum yields of electroluminescence from OSCs and decay kinetics of CT states, it is found that the radiative decay rate of CT states becomes larger when the energy offset is negligible compared with those in conventional OSCs with sufficient energy offset. This behavior is rationalized by hybridization between CT and local excited states, resulting in a considerable enhancement of the oscillator strength of CT states. Based on a trend observed in this study, the precise mechanism by which the energy offset affects the nonradiative voltage loss is discussed.

where  $q$  is the elementary charge). The voltage loss in OSCs is typically more than 0.7 V except for some state-of-the-art devices,<sup>[3–6]</sup> whereas it is only  $\approx 0.4$  V in Si-based solar cells.<sup>[7]</sup> This difference is partly because OSCs require donor–acceptor (DA) heterojunctions to ionize excitons.<sup>[8,9]</sup> At the DA interface, excitons separate as holes on the donor and electrons on the acceptor, forming charge transfer (CT) states with energies lower than  $E_g$ . Historically, it was thought that the energy offset between  $E_g$  and the CT state energy  $E_{CT}$  should be more than 0.3 eV for efficient charge generation.<sup>[4,10,11]</sup> However, recent studies have demonstrated efficient charge generation with a small energy offset.<sup>[12–16]</sup> Therefore, the voltage loss incurred by charge generation is no longer an unavoidable and intrinsic property of OSCs, although the mechanism of efficient charge generation without an energy offset remains unclear.

## 1. Introduction


The power conversion efficiency (PCE) of organic solar cells (OSCs) has been improving constantly over the past three decades because of the development of new donor and acceptor materials,<sup>[1]</sup> with some OSCs achieving  $>17\%$  PCEs.<sup>[2]</sup> However, the PCE of OSCs still lags behind that of their inorganic analogs. One remaining challenge in this field is to reduce the voltage loss  $\Delta V$ , which is defined as the difference between the optical bandgap energy  $E_g$  of a material and the open-circuit voltage ( $V_{OC}$ ) ( $\Delta V = E_g/q - V_{OC}$ ,

Another reason behind the voltage loss in OSCs is nonideal charge recombination. According to detailed balance theory, any type of solar cells will have unavoidable, intrinsic voltage loss relative to radiative charge recombination, even though there are no disorders or trap sites.<sup>[17]</sup> In the Shockley–Queisser (SQ) framework, the radiative recombination loss makes the upper limit of maximum achievable  $V_{OC}$  to be  $\approx 0.3$  V lower than  $E_g/q$ .<sup>[17,18]</sup> However, the voltage loss incurred by charge recombination in OSCs is significantly larger than the SQ limit, mainly because of an extra voltage loss caused by nonradiative charge recombination.<sup>[3–7,17–20]</sup> It has been experimentally demonstrated that CT states are intermediates of charge recombination in OSCs.<sup>[9,21]</sup> The oscillator strengths of CT states are fairly small because of poor spatial overlap between the highest occupied molecular orbital (HOMO) of the donor and lowest unoccupied molecular orbital (LUMO) of the acceptor, resulting in the radiative decay rate  $k_r$ , in general, being fairly smaller than the nonradiative decay rate  $k_{nr}$ . Therefore, the CT states predominantly decay nonradiatively to the ground state. The external quantum efficiency of electroluminescence (EQE<sub>EL</sub>) of OSCs is typically on the order of  $10^{-6}$ – $10^{-8}$ , which is equivalent to the nonradiative voltage loss  $\Delta V_{nr}$  of 0.35–0.46 V.<sup>[3,5–7,19,20,22]</sup> Therefore, OSCs with smaller  $\Delta V_{nr}$  are highly required.

Benduhn et al. found a negative correlation between  $\Delta V_{nr}$  and  $E_{CT}$ .<sup>[3]</sup> This is a clear signal of the energy gap law, or the transition rate in the Marcus inverted regime for the nonradiative transition of CT states to the ground state. In this regime, the

T. Saito, S. Natsuda, K. Imakita, Dr. Y. Tamai, Prof. H. Ohkita  
Department of Polymer Chemistry  
Graduate School of Engineering  
Kyoto University  
Katsura, Nishikyo, Kyoto 615-8510, Japan  
E-mail: tamai@photo.polym.kyoto-u.ac.jp

Dr. Y. Tamai  
Japan Science and Technology Agency (JST), PRESTO  
4-1-8 Honcho, Kawaguchi, Saitama 332-0012, Japan

 The ORCID identification number(s) for the author(s) of this article can be found under <https://doi.org/10.1002/solr.202000255>.

© 2020 The Authors. Published by WILEY-VCH Verlag GmbH & Co. KGaA, Weinheim. This is an open access article under the terms of the Creative Commons Attribution-NonCommercial-NoDerivs License, which permits use and distribution in any medium, provided the original work is properly cited, the use is non-commercial and no modifications or adaptations are made.

DOI: 10.1002/solr.202000255

nonradiative transition rate from the CT state with the lowest vibrational energy to an isoenergetic high vibrational ground state is proportional to the overlap between the vibrational wave functions of those states, which decreases with increasing difference in the vibrational quantum number.<sup>[23]</sup> Consequently, the nonradiative transition rate decreases exponentially with increasing  $E_{CT}$ ; hence,  $\Delta V_{nr}$  intrinsically increases linearly with decreasing  $E_{CT}$ .<sup>[3]</sup> On the contrary, there is a large variation in  $\Delta V_{nr}$  around the trend observed in ref. [3], indicating that other parameters also affect  $\Delta V_{nr}$ . Recently, Eisner et al. highlighted the importance of hybridizing local excited (LE) and CT states to reduce  $\Delta V_{nr}$ , based on their three-state model simulation.<sup>[24,25]</sup> They proposed that a hybrid LE–CT state is formed when the LE and CT states are very close in energy. Because the oscillator strength of the LE state is generally fairly larger than that of the CT state, the hybridization will result in a large enhancement in  $E_{QEL}$ . In contrast to their successful theoretical approach, there is a lack of experimental evidence of reducing nonradiative voltage loss through LE–CT hybridization.

Herein, we investigated the role of energy offset in nonradiative voltage loss in OSCs. We used PTB7-Th, which is a benchmark material for OSCs, as a common polymeric donor, and various fullerene and nonfullerene acceptors whose optical bandgaps are larger than that of PTB7-Th (the chemical structures of the materials used in this study are shown in **Figure 1**). In other words,  $E_g$  was determined based on that of PTB7-Th for all donor/acceptor blends, which makes our study very straightforward in discussing the role of energy offset in nonradiative voltage loss, as will be shown later. We found that the decrease in  $\Delta V_{nr}$  was considerably steeper than the general trend observed in ref. [3]. By measuring the  $E_{QEL}$  of OSCs and the decay kinetics of CT states using transient absorption (TA) spectroscopy, we found that the nonradiative recombination rate was less sensitive to either  $E_{CT}$  or the energy offset. Rather, the radiative recombination rate increased rapidly with decreasing energy offset. This behavior can be rationalized by the hybridization of LE and CT states, resulting in a considerable reduction of  $\Delta V_{nr}$  down to  $\approx 0.185$  V.

## 2. Results and Discussion

### 2.1. Energy Offset Ordering

**Figure 2** shows the current density–voltage ( $J$ – $V$ ) characteristics and photovoltaic external quantum efficiency ( $E_{QEPV}$ ) spectra of the solar cell devices used in this study (the photovoltaic device parameters are summarized in the Supporting Information). Note that the  $E_{QEPV}$  spectra were extended to lower energies using the EL spectra according to the previous report (the details are given in the Supporting Information).<sup>[7]</sup>  $E_g$  was determined from the  $E_{QEPV}$  spectra using the method proposed in ref. [26] wherein the first derivative of the  $E_{QEPV}$  spectrum is assumed to be a probability distribution function of the photovoltaic bandgap energy, and the mean value of distribution is used for  $E_g$ . We evaluated  $E_g$  to be approximately 1.65 eV, as summarized in **Table 1**, which is consistent with previous reports.<sup>[15,16]</sup> Acceptor materials were chosen to vary the LUMO energy offset from nearly zero to approximately 0.2 eV, according to the

literature values.<sup>[27]</sup> However, it is difficult to compare the reported LUMO values accurately because they strongly depend on the experimental methods. Moreover, it is well known that conventional experimental techniques often fail to provide correct LUMO energy levels because the energy level measured separately for each pristine film is often different from that near the buried interface in a bulk-heterojunction blend.<sup>[28]</sup> We need a more definitive criterion for the energy offset to understand its role in nonradiative voltage loss. Ideally, the energy offset should be quantified based on  $E_{CT}$ . However, estimating  $E_{CT}$  accurately from the absorption/emission band, which should appear on the lower energy side compared with that of bulk component, is more challenging because of a complete overlap with large bulk components when the offset is small or negligible. Instead, we temporarily provide a qualitative characterization of the energy offset here. Some devices exhibit clear shoulders in their  $E_{QEPV}$  spectra on the lower energy side, as shown in **Figure 2c**, clearly indicating the photocurrent response from the CT state absorption; this shoulder is negligible for other devices. From the  $E_{QEPV}$  spectra, the acceptor materials can be categorized into three groups: group I (sufficient offset group: PC<sub>71</sub>BM, di-PDI, and ITIC), group II (small offset group: bis-PCBM, IT-M, and IT-DM), and group III (negligible offset group: ICBA, IDT-2BR, and IDFBF). All these groups contain one fullerene and two nonfullerene acceptors, as shown in **Figure 1**. Additional quantitative characterization of the energy offset will be given later.

### 2.2. Quantifying the Radiative and Nonradiative Voltage Losses

Based on earlier studies,<sup>[7,18]</sup>  $V_{OC}$  can be divided into several components as follows

$$V_{OC} = V_{OC}^{SQ} - \Delta V_{SC} - \Delta V_r - \Delta V_{nr} = V_{OC}^{rad} - \Delta V_{nr} \quad (1)$$

$V_{OC}^{SQ}$  is derived from the SQ limit, which depends only on  $E_g$  and temperature. Its value is  $\approx 0.28$  V lower than  $E_g/q$  ( $E_g \approx 1.65$  eV) because of the unavoidable radiative charge recombination even in an ideal solar cell, as mentioned earlier.  $\Delta V_{SC}$ ,  $\Delta V_r$ , and  $\Delta V_{nr}$  are extra voltage losses associated with the nonideal behavior of real solar cells.  $\Delta V_{SC}$  is the extra voltage loss due to nonideal behavior above  $E_g$ , arising because  $E_{QEPV}$  is less than unity above  $E_g$ .  $\Delta V_r$  arises from nonideal behavior below  $E_g$ , being associated with a broadened  $E_{QEPV}$  tail that extends further below  $E_g$ , as shown in **Figure 2c**.  $\Delta V_{nr}$  is the extra voltage loss due to nonradiative charge recombination. On the right-hand side of Equation (1),  $V_{OC}^{rad}$  is the radiative open-circuit voltage of a solar cell, wherein radiative charge recombination is the only deactivation pathway. As will be shown later, we found  $V_{OC}^{rad}$  to be a good measure for quantitatively assessing the role of energy offset. **Table 1** shows the voltage losses of our devices (the details of the evaluation methods are given in the Supporting Information).

$\Delta V_{SC}$ , which ranges only from 16 to 26 mV, is typically much smaller than other losses because it is proportional to the logarithm of  $J_{SC}/J_{SC}^{SQ}$ , where  $J_{SC}$  is the short-circuit current density and  $J_{SC}^{SQ}$  is the maximum achievable  $J_{SC}$  in the SQ limit. An exception is the IDFBF device, where  $\Delta V_{SC}$  is relatively large (38 mV) because of poor photocurrent generation, as will be discussed later.  $\Delta V_r$  is strongly dependent on the

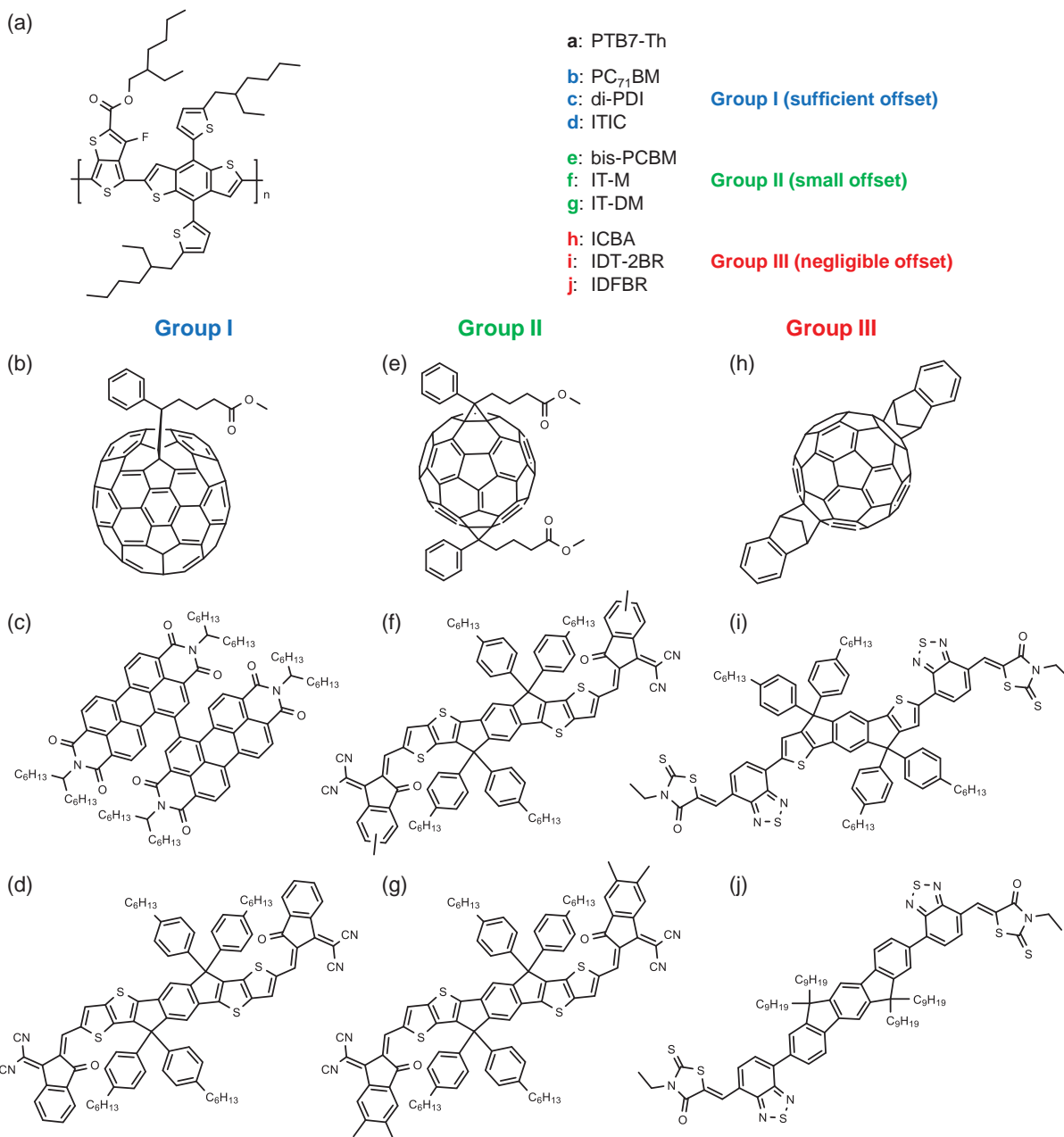


**Figure 1.** Chemical structures of PTB7-Th and various acceptor materials used in this study. The acceptor materials are categorized into three groups: group I (sufficient offset group: di-PDI, PC<sub>71</sub>BM, and ITIC), group II (small offset group: bis-PCBM, IT-M, and IT-DM), and group III (negligible offset group: ICBA, IDT-2BR, and IDFBR). Each group contains one fullerene and two nonfullerene acceptors.

choice of acceptor materials. Because  $\Delta V_r$  originates from the EQE<sub>PV</sub> tail below  $E_g$ , it contains losses from both the smeared-out absorption edge of the material ( $\Delta V_{r,1}$ ) and the CT state absorption ( $\Delta V_{r,2}$ ).<sup>[7]</sup> Because we used the common low-bandgap donor polymer in this study (i.e., the slope of the absorption edge of the bulk part for all devices should be almost constant), the variation in  $\Delta V_{r,1}$  originates from the variation in the photocurrent generation yields; because of the reciprocity relationship, a better EQE<sub>PV</sub> (i.e., a smaller  $\Delta V_{SC}$ ) results in larger radiative recombination (see the

Supporting Information for more details). In contrast,  $\Delta V_{r,2}$  is strongly dependent on the energy offset. As the intensity of the blackbody emission exponentially increases with decreasing energy, the weak shoulder of the EQE<sub>PV</sub> spectrum on the lower energy side, because of the weak CT state absorption, substantially contributes to the radiative recombination loss. We evaluated  $\Delta V_{r,1}$  and  $\Delta V_{r,2}$  separately, as shown in Table S2, Supporting Information, and found that  $\Delta V_{r,2}$  is suppressed to almost zero in group III, whereas it increases up to 100 mV in group I. Interestingly, there is a strong positive

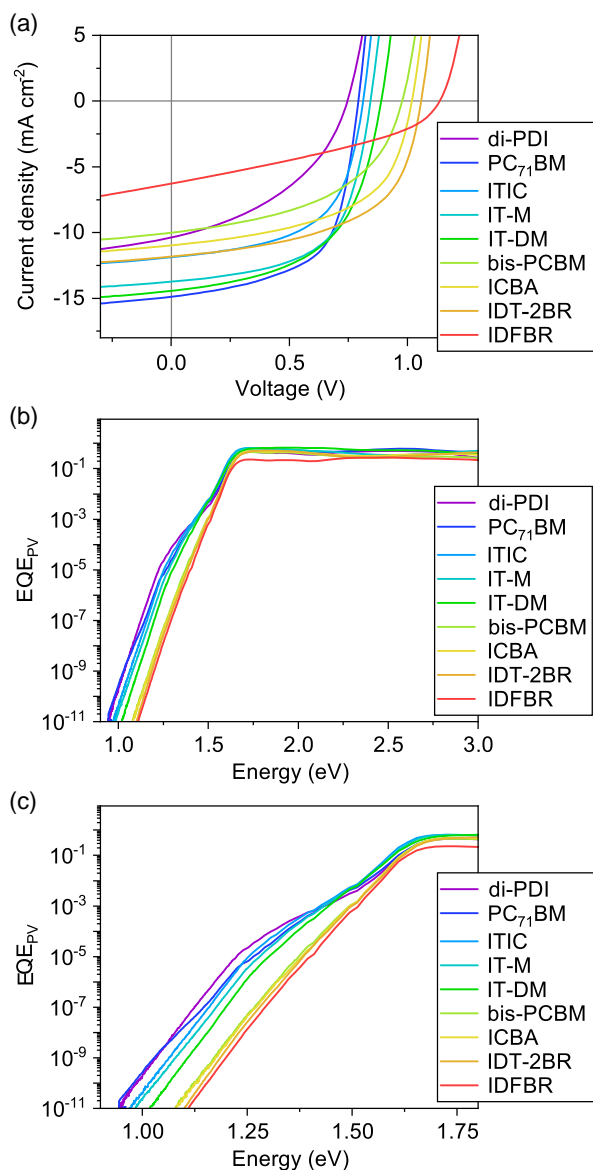


**Figure 2.** a)  $J$ - $V$  characteristics of photovoltaic devices. The device parameters are summarized in the Supporting Information. b)  $\text{EQE}_{\text{PV}}$  spectra of the devices extended to lower energies using the EL spectra. c) Enlarged image of panel b on the lower energy side.

**Table 1.** Various voltage losses for PTB7-Th/acceptor blend OSCs.

Group	Acceptor	$E_g$ [eV]	$\Delta V$ [V]	$V_{\text{OC}}^{\text{SQ}}$ [V]	$V_{\text{OC}}^{\text{rad}}$ [V]	$\Delta V_{\text{SC}}$ [V]	$\Delta V_r$ [V]	$\Delta V_{\text{nr}}$ [V]
I	di-PDI	1.646	0.898	1.372	1.187	0.023	0.162	0.439
	PC <sub>71</sub> BM	1.648	0.863	1.374	1.211	0.019	0.144	0.426
	ITIC	1.642	0.830	1.368	1.218	0.020	0.130	0.406
II	IT-M	1.645	0.799	1.370	1.235	0.018	0.117	0.389
	IT-DM	1.647	0.754	1.372	1.263	0.016	0.093	0.370
	bis-PCBM	1.645	0.673	1.371	1.294	0.026	0.051	0.322
III	ICBA	1.648	0.632	1.374	1.307	0.024	0.043	0.291
	IDT-2BR	1.648	0.592	1.374	1.312	0.023	0.039	0.256
	IDFBR	1.644	0.515	1.370	1.314	0.038	0.018	0.185

correlation between  $\Delta V_{\text{nr}}$  and  $\Delta V_r$ :  $\Delta V_{\text{nr}}$  decreases rapidly with decreasing  $\Delta V_r$ .

### 2.3. Impact of Energy Offset on Nonradiative Voltage Loss

As mentioned earlier, we need more quantitative characterization of the energy offset to discuss the role of energy offset in nonradiative voltage loss. As discussed in the Supporting Information, we found that  $V_{\text{OC}}^{\text{rad}}$  can be used as a good alternative to  $E_{\text{CT}}$ .  $V_{\text{OC}}^{\text{rad}}$  is expressed in terms of  $E_{\text{CT}}$  as follows

$$V_{\text{OC}}^{\text{rad}} = \frac{E_{\text{CT}}}{q} - \Delta V_{r,\text{bulk}} - \Delta V_{r,\text{CT}} \quad (2)$$

where  $\Delta V_{r,\text{bulk}} (= E_g/q - V_{\text{OC}}^{\text{SQ}} + \Delta V_{\text{SC}} + \Delta V_{r,1})$  is the radiative voltage loss associated with the photocurrent response caused by bulk absorption. As shown in Table S2, Supporting Information,  $\Delta V_{r,\text{bulk}}$  is less dependent on the choice of acceptor materials, for which the range is only  $0.355 \pm 0.015$  V, because we used the common low-bandgap donor in this study; hence, it can be assumed to be a constant (see the Supporting Information for more details). In contrast,  $\Delta V_{r,\text{CT}}$  is a function of CT state properties, which is defined as

$$\Delta V_{r,\text{CT}} = \Delta V_{r,2} - \frac{E_g - E_{\text{CT}}}{q} \quad (3)$$

However, what is critically important here is that although  $\Delta V_{r,\text{CT}}$  is clearly a function of the energy offset, its dependence is fairly modest because the former and latter terms of the right-hand side in Equation (3) cancel each other out, as discussed in the Supporting Information.  $\Delta V_{r,\text{CT}}$  remains almost constant when the energy offset is more than 50 meV, and it rapidly increases to zero when the offset approaches zero. In other words, we can assume that  $V_{\text{OC}}^{\text{rad}}$  is a direct measure of  $E_{\text{CT}}$ , at least for groups I and II, whereas it slightly underestimates  $E_{\text{CT}}$  for group III relative to groups I and II. We therefore plotted  $\Delta V_{\text{nr}}$  against  $V_{\text{OC}}^{\text{rad}}$ , as shown in Figure 3. In panel a, we also show  $\Delta V_{\text{nr}}$  over a span of previously published data.<sup>[3,7,13,29]</sup> The solid line in panel a represents the general trend for  $\Delta V_{\text{nr}}$  proposed in ref. [3] with a slope of  $-0.184 \text{ V V}^{-1}$ . This trend was described by the energy gap law based on the Marcus inverted regime for nonradiative transition rates in organic DA systems,<sup>[3]</sup>

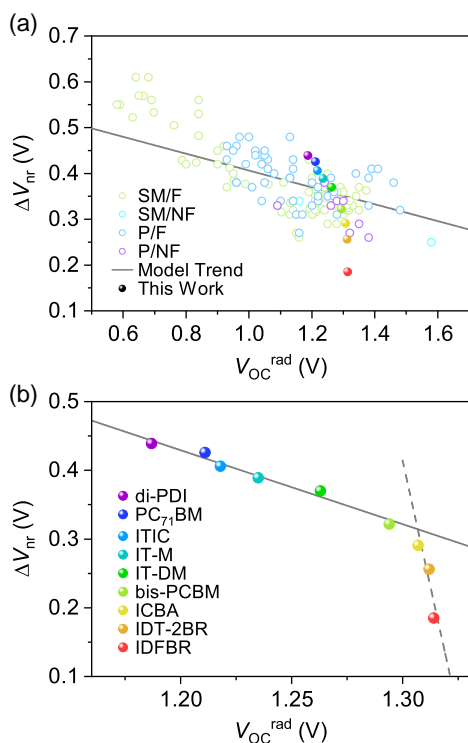


**Figure 3.** Nonradiative voltage loss  $\Delta V_{nr}$  as a function of the radiative open-circuit voltage  $V_{OC}^{rad}$ . Our results are shown as filled circles. In panel a, previously published data are also shown by open circles.<sup>[3,7,13,29]</sup> SM, small molecule donor; P, polymeric donor; F, fullerene acceptor; and NF, nonfullerene acceptor. The solid line in panel a represents the model trend proposed in ref. [3]. The solid and broken lines in panel b represent the trends observed in this study with slopes of  $-1.1$  and  $-14.6 \text{ V V}^{-1}$ , respectively.

suggesting that the large  $\Delta V_{nr}$  in OSCs is unavoidable as it is intrinsic to the C–C bond vibration in organic materials.

Although most of our results lie inside the scattered data set, as shown in Figure 3a, the trend we observed is clearly different from the general trend. Our results are extracted in panel b.  $\Delta V_{nr}$  decreased linearly with increasing  $V_{OC}^{rad}$ , regardless of whether we used fullerene or nonfullerene acceptors, exhibiting a slope of  $-1.1 \text{ V V}^{-1}$  (solid line in panel b), much steeper than that proposed in ref. [3] ( $-0.184 \text{ V V}^{-1}$ ). This finding emphasizes that  $\Delta V_{nr}$  significantly depends on other parameters as well as  $E_{CT}$ . Because we used a common low-bandgap donor (i.e., the  $E_g$  of all devices is almost constant),  $V_{OC}^{rad}$  can also be used as a direct measure of the energy offset, which is a key advantage of this study compared with previous reports. Our results indicate that  $\Delta V_{nr}$  decreases rapidly with decreasing energy offset. This is consistent with the model proposed in ref. [25] as will be discussed later.  $\Delta V_{nr}$  sharply deviates downward from the solid line when  $E_g/q - V_{OC}^{rad} < 0.35 \text{ V}$  ( $V_{OC}^{rad} > 1.3 \text{ V}$ ), where  $\Delta V_{nr}$  drops with a slope of  $-14.6 \text{ V V}^{-1}$ , as shown by the broken line in panel b. The minimum  $\Delta V_{nr}$  observed here is only 0.185 V for the IDFBR device, which is considerably small compared with other OSCs, as shown in Figure 3a, and comparable with those of inorganic analogs.<sup>[7,30]</sup> Note that the  $V_{OC}^{rad}$  in this region slightly underestimates the  $E_{CT}$  relative to the lower  $V_{OC}^{rad}$  region because

of negligible energy offset, as mentioned earlier. However, the key takeaway here is that a marginal decrease in energy offset significantly reduces  $\Delta V_{nr}$ .

## 2.4. Nonradiative Decay Kinetics

To confirm the large reduction in  $\Delta V_{nr}$  in group III, we measured the  $\text{EQE}_{EL}$  of the OSC devices because  $\Delta V_{nr}$  is directly related to  $\text{EQE}_{EL}$ , as follows

$$\Delta V_{nr} = \frac{k_B T}{q} \ln \left( \frac{1}{\text{EQE}_{EL}} \right) \quad (4)$$

where  $k_B$  and  $T$  are the Boltzmann constant and absolute temperature, respectively. Figure 4 shows the  $\text{EQE}_{EL}$  of our OSC devices plotted against applied voltage. The  $\text{EQE}_{EL}$  measured at two specific conditions, the  $\text{EQE}_{EL}(V_{OC})$  at which the applied bias was set at the  $V_{OC}$  and the  $\text{EQE}_{EL}(V_{J_{SC}})$  at which the current density was equivalent to the  $J_{SC}$ , is also shown in Table 2. As shown in Figure 4, the  $\text{EQE}_{EL}$  increased in order of the  $V_{OC}^{rad}$ . The  $\text{EQE}_{EL}$  for group I is on the order of  $10^{-6}$ – $10^{-8}$ , which is typical for conventional OSCs.<sup>[3,5–7,19,20,22]</sup> On the contrary, the  $\text{EQE}_{EL}$

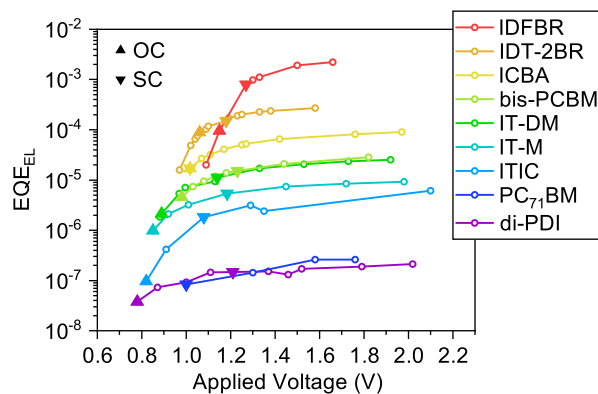


**Figure 4.**  $\text{EQE}_{EL}$  plotted against applied voltage.  $\blacktriangle$ , applied bias was set at the  $V_{OC}$  of each device;  $\blacktriangledown$ , applied bias was set at the  $V_{J_{SC}}$ , at which current density was equivalent to the  $J_{SC}$  of each device.

**Table 2.**  $\text{EQE}_{EL}$  from OSC devices.

Group	Acceptor	$\text{EQE}_{EL}(V_{OC})^a$	$\text{EQE}_{EL}(V_{J_{SC}})^b$
I	di-PDI	$3.8 \times 10^{-8}$	$1.5 \times 10^{-7}$
	PC <sub>71</sub> BM	n.a. <sup>c)</sup>	$8.3 \times 10^{-8}$
	ITIC	$9.7 \times 10^{-8}$	$1.8 \times 10^{-6}$
II	IT-M	$9.9 \times 10^{-7}$	$5.4 \times 10^{-6}$
	IT-DM	$2.2 \times 10^{-6}$	$1.1 \times 10^{-5}$
	bis-PCBM	$4.5 \times 10^{-6}$	$1.5 \times 10^{-5}$
III	ICBA	$1.7 \times 10^{-5}$	$1.7 \times 10^{-5}$
	IDT-2BR	$8.9 \times 10^{-5}$	$1.5 \times 10^{-4}$
	IDFBR	$9.6 \times 10^{-5}$	$7.9 \times 10^{-4}$

<sup>a)</sup>The applied bias was set at  $V_{OC}$ ; <sup>b)</sup>The applied bias was set at the  $V_{J_{SC}}$ , at which current density was equivalent to the  $J_{SC}$ ; <sup>c)</sup> $\text{EQE}_{EL}(V_{OC})$  of the PC<sub>71</sub>BM device was not available because the EL intensity was too weak.



for group III increased up to  $\approx 10^{-3}$ , which is three orders of magnitude larger than the conventional values.

$EQE_{EL}$  is mainly controlled by the internal photoluminescence (PL) quantum yield of CT states for OSCs, as follows

$$EQE_{EL} \sim \frac{k_r}{k_r + k_{nr}} \sim \frac{k_r}{k_{nr}} \quad (5)$$

Because the oscillator strengths of CT states are generally fairly small owing to a poor spatial overlap between the donor's HOMO and the acceptor's LUMO,  $k_r$  is significantly smaller than  $k_{nr}$ , resulting in extremely low  $EQE_{EL}$ , on the order of  $10^{-6}$ – $10^{-8}$ . This means that the large enhancement of  $EQE_{EL}$  in group III originates from either an enhancement in  $k_r$  or a reduction in  $k_{nr}$  in CT states.

To reveal the origin of the large enhancement, we monitored the decay kinetics of CT states using TA spectroscopy. Here, we measured a PTB7-Th/IDT-2BR blend film as a high- $EQE_{EL}$  material representing group III and a PTB7-Th/ITIC blend film as a low- $EQE_{EL}$  counterpart representing group I. **Figure 5a** shows the TA spectra of the PTB7-Th/ITIC blend film. The sharp photoinduced absorption (PIA) and broad PIA bands observed immediately after photoexcitation at approximately 950 and 1400 nm are assigned to singlet excitons of ITIC and PTB7-Th, respectively, as reported previously.<sup>[31,32]</sup> The negative signals below 800 nm are attributable to the ground state bleaching (GSB) of the blend film. The singlet excitons monitored at

1400 nm decayed with a time constant of 2.5 ps (panel c), whereas a broad PIA band ranging from 900 to 1200 nm was also observed, which is assigned to ITIC radical anions (peaking at approximately 950 nm) and PTB7-Th hole polarons (peaking at approximately 1150 nm).<sup>[31,32]</sup> At a later time stage, a new PIA signal at approximately 1300 nm, which is assigned to triplet excitons of PTB7-Th generated through bimolecular charge recombination,<sup>[31]</sup> became more pronounced. On the contrary, **Figure 5b** shows the TA spectra of the PTB7-Th/IDT-2BR blend film. Following photoexcitation, a broad PIA signal attributable to the superimposition of singlet excitons of PTB7-Th (1400 nm) and IDT-2BR (1200 nm) was observed. As in the case of the ITIC blend, singlet excitons were then converted into charged species, peaking at approximately 1150 nm. Singlet excitons decayed more slowly compared with that in the ITIC blend with a time constant of 38 ps as will be discussed later. Note that the PIA band of IDT-2BR radical anions was not observed, probably because of the small absorption cross section. Triplet excitons of PTB7-Th (1300 nm) were also observed in this blend. On the contrary, because we aim to monitor the decay kinetics of CT states through geminate recombination to the ground state, bimolecular recombination should be suppressed. As shown in the Supporting Information, the decay kinetics of PTB7-Th hole polarons were independent of the excitation intensity under  $0.8 \mu\text{J cm}^{-2}$ , indicating the absence of bimolecular recombination below  $0.8 \mu\text{J cm}^{-2}$ . Under such a weak excitation, the polaron signals decayed monoexponentially with time constants

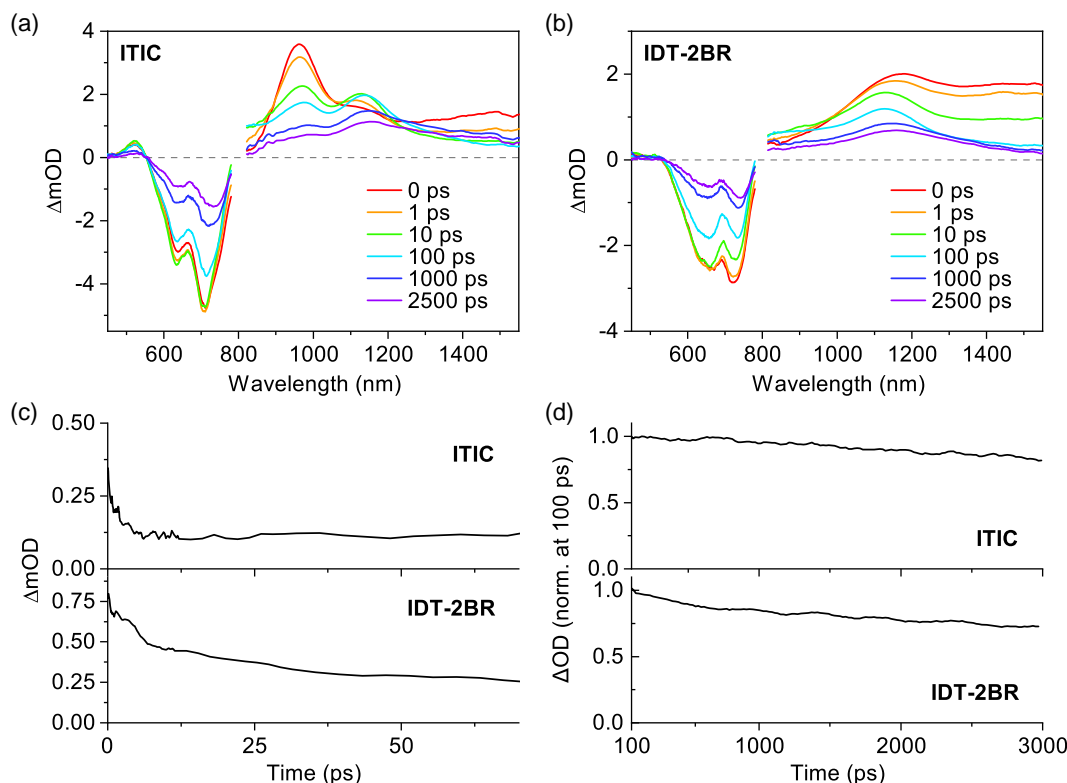


**Figure 5.** TA spectra of a) PTB7-Th/ITIC and b) PTB7-Th/IDT-2BR blends. The excitation wavelength was set at 650 nm with a fluence of  $2.4 \mu\text{J cm}^{-2}$ . c) Time evolution of exciton signals with a fluence of  $0.8 \mu\text{J cm}^{-2}$  monitored at 1400 nm. d) Time evolution of polaron signals with a fluence of  $0.8 \mu\text{J cm}^{-2}$  monitored at 1150 nm. The TA signals were normalized at 100 ps.

of  $\approx 1.9$  and  $\approx 1.3$  ns for the ITIC and IDT-2BR blends, respectively, as shown in panel d (TA spectra under the weak excitation are shown in the Supporting Information). These values are on the same order as those reported previously for PC<sub>71</sub>BM and di-PDI blends.<sup>[31]</sup> Because the EQE<sub>EL</sub> of these devices is significantly lower than unity, we can safely assume that  $k_{nr}$  is the inverse of the CT state lifetime; hence,  $k_{nr}$  was evaluated to be  $\approx 5.3 \times 10^8 \text{ s}^{-1}$  and  $\approx 7.7 \times 10^8 \text{ s}^{-1}$  for the ITIC and IDT-2BR blends, respectively. This indicates that the nonradiative transition rate is less sensitive to either  $E_{CT}$  or the energy offset. Rather, it would depend on other parameters such as morphology near the DA interface or the electronic coupling matrix element of electrons and holes. Therefore, the fact that the EQE<sub>EL</sub> observed in the IDT-2BR device is three orders of magnitude larger than that of the ITIC device cannot be explained by the reduction in  $k_{nr}$ .

### 2.5. Hybridization of LE and CT States

In the previous section, we demonstrated that the large enhancement in EQE<sub>EL</sub> observed in group III cannot be rationalized by the decrease in  $k_{nr}$ . This means that  $k_r$  is much larger for the CT states in group III than those in group I. In fact, the  $k_r$  was roughly estimated based on the EQE<sub>EL</sub> and  $k_{nr}$  to be  $\approx 10^5$  and  $\approx 10^2 \text{ s}^{-1}$  for the IDT-2BR and ITIC blends, respectively. Recently, Eisner et al. proposed that a hybrid LE–CT state is formed when the LE and CT states are very close in energy.<sup>[24,25]</sup> Once the hybrid states are formed, the oscillator strength of the CT states is enhanced by the hybridization of a certain degree with the nearest donor or acceptor. Owing to negligible energy offset in group III, the  $E_{CT}$  of these blends should be very close to  $E_g$ , resulting in the formation of hybrid LE–CT states with significantly larger  $k_r$ . This study provides clear experimental evidence on the role of energy offset in nonradiative voltage loss. The energy offset affects not only the voltage loss incurred by charge generation ( $E_g - E_{CT}$ )/ $q$ , but also  $\Delta V_{nr}$  by enhancing the oscillator strength of the CT states.

Importantly, we could not find any intrinsic differences in  $\Delta V_{nr}$  between the fullerene and nonfullerene acceptors in groups I and II, wherein  $\Delta V_{nr}$  decreases linearly with decreasing energy offset without a large deviation, as shown in Figure 3b. Note that because we used the common low-bandgap donor polymer, variations in PL quantum yields of the acceptor materials have no impact on  $\Delta V_{nr}$  in this study, while it would significantly affect  $\Delta V_{nr}$  when we use low-bandgap acceptors. The trend we observed has a slope of  $-1.1 \text{ V V}^{-1}$  (solid line in Figure 3b), meaning that a small reduction in energy offset by only 50 meV produces a large enhancement in EQE<sub>EL</sub> by nearly one order of magnitude.  $\Delta V_{nr}$  in group III, where the difference between  $V_{OC}^{SQ}$  and  $V_{OC}^{rad}$  is less than 70 mV, drops more rapidly (slope of  $-14.6 \text{ V V}^{-1}$ , broken line in Figure 3b). Consequently, a 130 mV increase in  $V_{OC}^{rad}$  (from di-PDI to IDFBR) results in a 250 mV reduction in  $\Delta V_{nr}$ . Because a change in energy offset by 100 meV often occurs at the DA interface even when we use the same donor/acceptor materials as reported previously,<sup>[28]</sup> our findings emphasize the importance of fine-tuning the energy landscape near the DA interface. Interestingly, in contrast to groups I and II, no fullerene acceptor that deviates considerably

from the solid line in Figure 3b was observed in this study (ICBA sits close to the intersection). This result implies that nonfullerene acceptors may be intrinsically advantageous in reducing the nonradiative voltage loss, although the limited data set presented herein is insufficient to obtain an unambiguous conclusion. Nevertheless, nonfullerene acceptors are clearly better candidates for further improvement because of the easier optimization of HOMO and LUMO energies.

One drawback of reducing the energy offset is that a smaller energy offset often leads to slow and inefficient charge separation.<sup>[14,16,33]</sup> For example, Li et al. found a strong correlation between LUMO energy offset and EQE<sub>PV</sub>, with EQE<sub>PV</sub> dropping sharply when  $\Delta V$  was less than 0.6 V because of a poor charge separation efficiency.<sup>[34]</sup> We also observed a slower CT in the IDT-2BR blend, as shown in Figure 5c. Singlet excitons in the IDT-2BR blend decayed more slowly than those in the ITIC blend. According to the Marcus theory for electron transfer in the normal regime, CT at the DA interface becomes slower with decreasing energy offset. This may lead to inefficient CT when the energy offset is negligible. On the contrary, the IDT-2BR blend showed a PL quenching efficiency of  $\approx 90\%$  (see the Supporting Information), indicating that excitons dissociate slowly yet efficiently without an energy offset in the IDT-2BR blend. In contrast, approximately 60% of excitons did not dissociate into CT states in the IDFBR blend (see the Supporting Information), although the  $\Delta V_{nr}$  was the smallest, resulting in the lowest EQE<sub>PV</sub> and PCE in our devices. These results may allow a compromise when reducing the energy offset. On the contrary, sub-picosecond ultrafast CT with near-zero energy offset was observed very recently in some donor/acceptor blends.<sup>[35]</sup> Because the mechanism of ultrafast CT without an energy offset remains unclear, further spectroscopic studies are highly required. Another option to overcome this tradeoff has been recently suggested by some authors of this study,<sup>[32]</sup> using a thienoazacoronene-based novel nonfullerene acceptor called TACIC. This acceptor shows an extremely long exciton lifetime of 1.59 ns in the film state as opposed to a relatively low  $E_g$  of 1.59 eV, allowing an efficient exciton dissociation efficiency ( $>95\%$ ) and EQE<sub>PV</sub> ( $\approx 80\%$ ), despite slow charge generation ( $\approx 60$  ps).

### 3. Conclusion

We have investigated the role of energy offset in nonradiative voltage loss  $\Delta V_{nr}$  in OSCs composed of PTB7-Th as a common donor and various fullerene and nonfullerene acceptors. As we utilized the common low-bandgap donor, we could use the radiative open-circuit voltage  $V_{OC}^{rad}$  as a direct measure of both  $E_{CT}$  and the energy offset. We observed that the nonradiative voltage loss reduced very rapidly with decreasing energy offset. The plot of  $\Delta V_{nr}$  against CT state energy  $E_{CT}$  ( $V_{OC}^{rad}$ ) had a slope of  $-1.1 \text{ V eV}^{-1}$ , which is much steeper than the general trend described by the energy gap law based on the Marcus inverted regime for nonradiative transition rates in organic DA systems. The variation observed in previous reports is attributable to the fact that the energy difference between  $E_g$  and  $E_{CT}$  is more important than  $E_{CT}$  itself for  $\Delta V_{nr}$ . This indicates that we can achieve a small  $\Delta V_{nr}$  with a low  $E_{CT}$  as opposed to the energy gap law.

From  $\text{EQE}_{\text{EL}}$  and TA measurements, we conclude that the nonradiative transition rate  $k_{\text{nr}}$  is less sensitive to either  $E_{\text{CT}}$  or the energy offset, whereas the radiative recombination rate  $k_r$  increases rapidly with decreasing energy offset. This is rationalized by the hybridization of LE and CT states. When the LE and CT states are very close in energy, hybrid LE–CT states are formed, enhancing the oscillator strength of the CT states. The trend observed in this study indicates that a small reduction in the energy offset by only 50 meV produces a large enhancement in  $\text{EQE}_{\text{EL}}$  by nearly one order of magnitude, emphasizing the importance of fine-tuning the energy landscape near the DA interface. A drawback associated with energy offset reduction may be slow and inefficient charge generation. Therefore, non-fullerene acceptors with very long exciton lifetimes would be good candidates for overcoming this problem and simultaneously achieving efficient charge generation and small  $\Delta V_{\text{nr}}$  to further improve OSCs.

## Supporting Information

Supporting Information is available from the Wiley Online Library or from the author.

## Acknowledgements

This work was partly supported by JST PRESTO program grant number JPMJPR1874, JSPS KAKENHI Grant-in-Aid for Young Scientists (B) No. 17K14527 and The Murata Science Foundation.

## Conflict of Interest

The authors declare no conflict of interest.

## Keywords

charge recombination, charge transfer state, energy loss, open-circuit voltage, polymer solar cells

Received: May 19, 2020

Revised: June 8, 2020

Published online: June 21, 2020

- [1] a) L. Lu, T. Zheng, Q. Wu, A. M. Schneider, D. Zhao, L. Yu, *Chem. Rev.* **2015**, *115*, 12666; b) J. Hou, O. Inganäs, R. H. Friend, F. Gao, *Nat. Mater.* **2018**, *17*, 119; c) A. Wadsworth, M. Moser, A. Marks, M. S. Little, N. Gasparini, C. J. Brabec, D. Baran, I. McCulloch, *Chem. Soc. Rev.* **2019**, *48*, 1596; d) H. Fu, Z. Wang, Y. Sun, *Angew. Chem. Int. Ed.* **2019**, *58*, 4442; e) Z. Zheng, H. Yao, L. Ye, Y. Xu, S. Zhang, J. Hou, *Mater. Today*, *35*, 115.
- [2] a) L. Meng, Y. Zhang, X. Wan, C. Li, X. Zhang, Y. Wang, X. Ke, Z. Xiao, L. Ding, R. Xia, H.-L. Yip, Y. Cao, Y. Chen, *Science* **2018**, *361*, 1094; b) Y. Lin, B. Adilbekova, Y. Firdaus, E. Yengel, H. Faber, M. Sajjad, X. Zheng, E. Yarali, A. Seitkhan, O. M. Bakr, A. El-Labban, U. Schwingenschlög, V. Tung, I. McCulloch, F. Laquai, T. D. Anthopoulos, *Adv. Mater.* **2019**, *31*, 1902965; c) Q. Liu, Y. Jiang, K. Jin, J. Qin, J. Xu, W. Li, J. Xiong, J. Liu, Z. Xiao, K. Sun, S. Yang, X. Zhang, L. Ding, *Sci. Bull.* **2020**, *65*, 272.
- [3] J. Benduhn, K. Tvingstedt, F. Piersimoni, S. Ullbrich, Y. Fan, M. Tropiano, K. A. McGarry, O. Zeika, M. K. Riede, C. J. Douglas, S. Barlow, S. R. Marder, D. Neher, D. Spoltore, K. Vandewal, *Nat. Energy* **2017**, *2*, 17053.
- [4] S. M. Menke, N. A. Ran, G. C. Bazan, R. H. Friend, *Joule* **2018**, *2*, 25.
- [5] M. Azzouzi, T. Kirchartz, J. Nelson, *Trends Chem.* **2019**, *1*, 49.
- [6] K. Vandewal, S. Mertens, J. Benduhn, Q. Liu, *J. Phys. Chem. Lett.* **2020**, *11*, 129.
- [7] J. Yao, T. Kirchartz, M. S. Vezie, M. A. Faist, W. Gong, Z. He, H. Wu, J. Troughton, T. Watson, D. Bryant, J. Nelson, *Phys. Rev. Appl.* **2015**, *4*, 014020.
- [8] a) T. M. Clarke, J. R. Durrant, *Chem. Rev.* **2010**, *110*, 6736; b) H. Ohkita, S. Ito, *Polymer* **2011**, *52*, 4397; c) F. Gao, O. Inganäs, *Phys. Chem. Chem. Phys.* **2014**, *16*, 20291; d) H. Ohkita, Y. Tamai, H. Benten, S. Ito, *IEEE J. Sel. Top. Quantum Electron.* **2016**, *22*, 100; e) Y. Tamai, *Polym. J.*, *10*, 1035.
- [9] K. Vandewal, *Annu. Rev. Phys. Chem.* **2016**, *67*, 113.
- [10] J.-L. Brédas, D. Beljonne, V. Coropceanu, J. Cornil, *Chem. Rev.* **2004**, *104*, 4971.
- [11] R. A. J. Janssen, J. Nelson, *Adv. Mater.* **2013**, *25*, 1847.
- [12] a) M. Wang, H. Wang, T. Yokoyama, X. Liu, Y. Huang, Y. Zhang, T.-Q. Nguyen, S. Aramaki, G. C. Bazan, *J. Am. Chem. Soc.* **2014**, *136*, 12576; b) K. Kawashima, Y. Tamai, H. Ohkita, I. Osaka, K. Takimiya, *Nat. Commun.* **2015**, *6*, 10085; c) S. M. Menke, A. Cheminal, P. Conaghan, N. A. Ran, N. C. Greeham, G. C. Bazan, T. Q. Nguyen, A. Rao, R. H. Friend, *Nat. Commun.* **2018**, *9*, 277; d) L. Perdigon-Toro, H. Zhang, A. Markina, J. Yuan, S. M. Hosseini, C. M. Wolff, G. Zuo, M. Stolterfoht, Y. Zou, F. Gao, D. Andrienko, S. Shoaee, D. Neher, *Adv. Mater.* **2020**, *32*, 1906763; e) S. Liu, J. Yuan, W. Deng, M. Luo, Y. Xie, Q. Liang, Y. Zou, Z. He, H. Wu, Y. Cao, *Nat. Photonics* **2020**, *14*, 300.
- [13] J. Liu, S. Chen, D. Qian, B. Gautam, G. Yang, J. Zhao, J. Bergqvist, F. Zhang, W. Ma, H. Ade, O. Inganäs, K. Gundogdu, F. Gao, H. Yan, *Nat. Energy* **2016**, *1*, 16089.
- [14] S. Li, L. Zhan, C. Sun, H. Zhu, G. Zhou, W. Yang, M. Shi, C.-Z. Li, J. Hou, Y. Li, H. Chen, *J. Am. Chem. Soc.* **2019**, *141*, 3073.
- [15] M. E. Ziffer, S. B. Jo, H. Zhong, L. Ye, H. Liu, F. Lin, J. Zhang, X. Li, H. W. Ade, A. K. Y. Jen, D. S. Ginger, *J. Am. Chem. Soc.* **2018**, *140*, 9996.
- [16] D. Qian, Z. Zheng, H. Yao, W. Tress, T. R. Hopper, S. Chen, S. Li, J. Liu, S. Chen, J. Zhang, X.-K. Liu, B. Gao, L. Ouyang, Y. Jin, G. Pozina, I. A. Buyanova, W. M. Chen, O. Inganäs, V. Coropceanu, J.-L. Brédas, H. Yan, J. Hou, F. Zhang, A. A. Bakulin, F. Gao, *Nat. Mater.* **2018**, *17*, 703.
- [17] W. Shockley, H. J. Queisser, *J. Appl. Phys.* **1961**, *32*, 510.
- [18] U. Rau, *Phys. Rev. B* **2007**, *76*, 085303.
- [19] M. Azzouzi, J. Yan, T. Kirchartz, K. Liu, J. Wang, H. Wu, J. Nelson, *Phys. Rev. X* **2018**, *8*, 031055.
- [20] K. D. Rosenthal, M. P. Hughes, B. R. Luginbuhl, N. A. Ran, A. Karki, S. J. Ko, H. Hu, M. Wang, H. Ade, T.-Q. Nguyen, *Adv. Energy Mater.* **2019**, *9*, 1901077.
- [21] a) K. Tvingstedt, K. Vandewal, A. Gadisa, F. Zhang, J. Manca, O. Inganäs, *J. Am. Chem. Soc.* **2009**, *131*, 11819; b) C. Deibel, T. Strobel, V. Dyakonov, *Adv. Mater.* **2010**, *22*, 4097; c) G. Lakhwani, A. Rao, R. H. Friend, *Annu. Rev. Phys. Chem.* **2014**, *65*, 557.
- [22] a) K. Tvingstedt, J. V. Manca, O. Inganäs, A. Gadisa, K. Vandewal, *Nat. Mater.* **2009**, *8*, 904; b) K. Vandewal, K. Tvingstedt, A. Gadisa, O. Inganäs, J. V. Manca, *Phys. Rev. B* **2010**, *81*, 125204.
- [23] R. Englman, J. Jortner, *Mol. Phys.* **1970**, *18*, 145.
- [24] X.-K. Chen, V. Coropceanu, J.-L. Brédas, *Nat. Commun.* **2018**, *9*, 5295.
- [25] F. D. Eisner, M. Azzouzi, Z. Fei, X. Hou, T. D. Anthopoulos, T. J. S. Dennis, M. Heeney, J. Nelson, *J. Am. Chem. Soc.* **2019**, *141*, 6362.



- [26] U. Rau, B. Blank, T. C. M. Müller, T. Kirchartz, *Phys. Rev. Appl.* **2017**, *7*, 044016.
- [27] a) M. Lenes, G.-J. A. H. Wetzelaer, F. B. Kooistra, S. Veenstra, J. C. Hummelen, P. W. M. Blom, *Adv. Mater.* **2008**, *20*, 2116; b) Y. Lin, J. Wang, Z. G. Zhang, H. Bai, Y. Li, D. Zhu, X. Zhan, *Adv. Mater.* **2015**, *27*, 1170; c) J. Zhao, Y. Li, H. Lin, Y. Liu, K. Jiang, C. Mu, T. Ma, J. Y. Lin Lai, H. Hu, D. Yu, H. Yan, *Energy Environ. Sci.* **2015**, *8*, 520; d) P. Cheng, M. Zhang, T. K. Lau, Y. Wu, B. Jia, J. Wang, C. Yan, M. Qin, X. Lu, X. Zhan, *Adv. Mater.* **2017**, *29*, 1605216; e) D. Baran, R. S. Ashraf, D. A. Hanifi, M. Abdelsamie, N. Gasparini, J. A. Röhr, S. Holliday, A. Wadsworth, S. Lockett, M. Neophytou, C. J. M. Emmott, J. Nelson, C. J. Brabec, A. Amassian, A. Salleo, T. Kirchartz, J. R. Durrant, I. McCulloch, *Nat. Mater.* **2017**, *16*, 363; f) F. Zhao, Y. Li, Z. Wang, Y. Yang, Z. Wang, G. He, J. Zhang, L. Jiang, T. Wang, Z. Wei, W. Ma, B. Li, A. Xia, Y. Li, C. Wang, *Adv. Energy Mater.* **2017**, *7*, 1602552; g) W. Huang, E. Y. B. Cheng, Y. Yang, C. R. McNeill, *Adv. Energy Mater.* **2017**, *7*, 1602197.
- [28] a) F. C. Jamieson, E. B. Domingo, T. McCarthy-Ward, M. Heaney, N. Stingelin, J. R. Durrant, *Chem. Sci.* **2012**, *3*, 485; b) S. Sweetnam, K. R. Graham, G. O. Ngongang Ndjawa, T. Heumüller, J. A. Bartelt, T. M. Burke, W. Li, W. You, A. Amassian, M. D. McGehee, *J. Am. Chem. Soc.* **2014**, *136*, 14078; c) H. Cha, G. Fish, J. Luke, A. Alraddadi, H. H. Lee, W. Zhang, Y. Dong, S. Limbu, A. Wadsworth, L. P. Maria, L. Francàs, H. L. Sou, T. Du, J.-S. Kim, M. A. McLachlan, I. McCulloch, J. R. Durrant, *Adv. Energy Mater.* **9**, 1901254.
- [29] a) S. M. Tuladhar, M. Azzouzi, F. Delval, J. Yao, A. A. Y. Guilbert, T. Kirchartz, N. F. Montcada, R. Dominguez, F. Langa, E. Palomares, J. Nelson, *ACS Energy Lett.* **2016**, *1*, 302; b) D. Baran, T. Kirchartz, S. Wheeler, S. Dimitrov, M. Abdelsamie, J. Gorman, R. S. Ashraf, S. Holliday, A. Wadsworth, N. Gasparini, P. Kaienburg, H. Yan, A. Amassian, C. J. Brabec, J. R. Durrant, I. McCulloch, *Energy Environ. Sci.* **2016**, *9*, 3783; c) Z. Fei, F. D. Eisner, X. Jiao, M. Azzouzi, J. A. Röhr, Y. Han, M. Shahid, A. S. R. Chesman, C. D. Easton, C. R. McNeill, T. D. Anthopoulos, J. Nelson, M. Heaney, *Adv. Mater.* **2018**, *30*, 1705209.
- [30] Y. Wang, Y. Wang, L. Zhu, H. Liu, J. Fang, X. Guo, F. Liu, Z. Tang, M. Zhang, Y. Li, *Energy Environ. Sci.* **2020**, *13*, 1309.
- [31] Y. Tamai, Y. Fan, V. O. Kim, K. Ziabrev, A. Rao, S. Barlow, S. R. Marder, R. H. Friend, S. M. Menke, *ACS Nano* **2017**, *11*, 12473.
- [32] T. Umeyama, K. Igarashi, D. Sasada, Y. Tamai, K. Ishida, T. Koganezawa, S. Ohtani, K. Tanaka, H. Ohkita, H. Imahori, *Chem. Sci.* **2020**, *11*, 3250.
- [33] a) E. T. Hoke, K. Vandewal, J. A. Bartelt, W. R. Mateker, J. D. Douglas, R. Noriega, K. R. Graham, J. M. J. Fréchet, A. Salleo, M. D. McGehee, *Adv. Energy Mater.* **2013**, *3*, 220; b) S. Holliday, R. S. Ashraf, A. Wadsworth, D. Baran, S. A. Yousaf, C. B. Nielsen, C.-H. Tan, S. D. Dimitrov, Z. Shang, N. Gasparini, M. Alamoudi, F. Laquai, C. J. Brabec, A. Salleo, J. R. Durrant, I. McCulloch, *Nat. Commun.* **2016**, *7*, 11585.
- [34] W. Li, K. H. Hendriks, A. Furlan, M. M. Wienk, R. A. J. Janssen, *J. Am. Chem. Soc.* **2015**, *137*, 2231.
- [35] Y. Zhong, M. Causa, G. J. Moore, P. Krauspe, B. Xiao, F. Gunther, J. Kublitski, R. Shivhare, J. Benduhn, E. BarOr, S. Mukherjee, K. M. Yallum, J. Rehault, S. C. B. Mannsfeld, D. Neher, L. J. Richter, D. M. DeLongchamp, F. Ortmann, K. Vandewal, E. Zhou, N. Banerji, *Nat. Commun.* **2020**, *11*, 833.